STRUCTURALLY STITCHED PREFORMS: EXPERIMENTAL CHARACTERIZATION, GEOMETRICAL MODELLING, AND FE ANALYSIS

V. Koissin[†], J. Kustermans[†], S.V. Lomov[*†], I. Verpoest[†],
H. Nakai[‡], T. Kurashiki[‡], K. Hamada[‡], Y. Momoji[‡], and M. Zako[‡]

[†] Dept. of Metallurgy and Materials Engineering, Katholieke Universiteit Leuven,
Kasteelpark Arenberg 44, B–3001 Heverlee, Belgium
[‡] Graduate School of Engineering, Osaka University,
2-1 Yamadaoka, Suita, Osaka 565–0871, Japan
[*]Stepan.Lomov@mtm.kuleuven.be

ABSTRACT

In this study, experimental data, geometrical models, and FE analysis are presented for typical structurally stitched multilayer preform composed of quasi-UD carbon-fibre woven fabric. The term 'structural' presumes here that the stitching yarn does not only consolidate the plies (as the non-structural one does) but forms also a through-the-thickness reinforcement. One stitching technique — tufting — is studied, with 67 tex carbon yarn. The models account for general features of the local preform geometry and are believed to allow for a sufficient modelling on the meso-scale (textile unit cell) level. Experimental and theoretical results are presented, compared and discussed; a "road" map is proposed for the modelling of structurally stitched preforms.

1. INTRODUCTION

It is well-known that a significant variability can exists in the internal geometry of a textile composite [1]. Particularly, this is the case for the structurally stitched preforms. The fibre placement is not uniform even in a raw material (fibre tows or yarns). Then, the needles of a knitting device (for NCF's) or a textile process still more increase this non-uniformity of the fibre content. While stitching structurally (i.e. with a relatively thick and firm yarn), the fibres are again pushed aside the needle; a breakage and vertical movement (crimpling) of some fibres can also be induced [2]. During the forming and compression in a mould, the fibre distribution is changed again. Finally, the micro- and meso-structure of a composite part can differ very much from that of the raw fabric.

Variability of the internal structure includes also random nesting of layers, random overlap of the "structural" and "non-structural" piercing patterns and openings (for NCF's), wide distribution of the opening dimensions, etc. [2, 3]. As a result, the composite has a complex hierarchical (meso- and micro-) structure having a significant randomization. The meso level (0.1–100 mm) includes the yarn loops (non-structural and structural), openings in the fibrous plies, gaps between the plies, etc. The micro level (10–100 μm) embraces the variable fibre content in a ply and yarn. Then, an investigation is difficult due to a bulk of parameters (stitching method/speed, distance between stitches/seams, dimension of the needle, properties of the preform/yarn, yarn tension, etc.). The modelling is thus sophisticated and case-dependent, and a broad experience is wanted.

The present study aims at a generalized meso-scale modelling approach suitable for the engineering purposes. The focus is laid on theoretical (method of inclusions) and FE estimation of the homogenized mechanical properties. Damage onset is also considered.

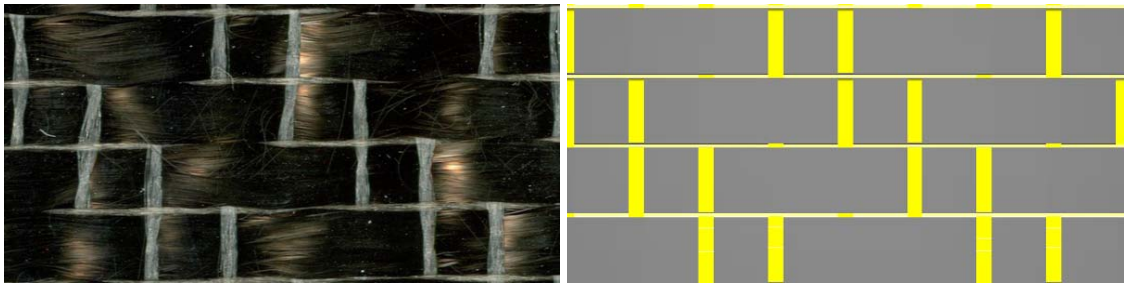

Figure 1: The woven fabric (left) and its geometrical model built using WiseTex (right).

Figure 2: Face side (left) and backside (right) of the stitched preform.

2. MATERIALS

Quasi-UD hybrid woven fabric (warp: 24K carbon tows alternated with thin polysulfone yarns; weft: the same polysulfone yarns) with the total areal weight of 226 g/m^2 is used as the raw material, Fig. 1. The areal weight of the carbon tows is 200 g/m^2.

To characterize the meso-geometry, the fabric surface is scanned, and about 50 lines are marked in a separate image layer for each dimension (yarn width, spacing). The layer is saved as a bitmap file and committed to a Matlab applet, which searches for the marked lines and calculated their lengths. Finally, the average values and standard deviations are assessed. For the carbon tows, the measured width is 4.34$\pm$0.14 mm that agrees well with the manufacturer's data [4] — 6$\pm$0.5 ends per inch or 4.23 mm. For the polysulfone yarn, the measured width is 0.22$\pm$0.0 mm (warp) or 0.91$\pm$0.18 mm (weft) that also agrees well with the datasheet (6$\pm$0.5 ends and 6$\pm$1 picks per inch).

The fabric was composed of 28 plies having symmetric stacking sequence [90°/45°/0°/0°/-45°/90°/-45°/0°/0°/45°/0°/-45°/0°/45°]$_s$, where 90° corresponds to the warp (carbon fibre) direction in the surface plies, i.e. to the horizontal direction in Fig. 1.

For the structural stitching, 1K carbon yarn [5] and the tufting method (KL RS 522 stitching head mounted on a KUKA-robot) are employed. The machine direction coincides with 0° direction of the preform. The piercing pattern is square 5x5 mm; the backside loop height is also about 5 mm. Typical photos of the stitched preform are shown in Fig. 2.

During the tufting, fiber-free zones (called "openings") appear around the stitching sites; these openings are naturally oriented along the global fibre orientation in the ply. Their geometrical characterization is performed in the same way as described above for the fabric structure; results are given in Table 1. Since the backside openings almost hide under numerous yarn loops, Fig. 2(right), they are cut off within a small area sufficient for the measurements. The backside loops show a relatively wide distribution in width and height; this is obviously due to the fact that these parameters are hardly controlled during the tufting and much influenced by the natural friction between the plies and yarn.

Table 1: *Measured dimensions of the "openings" and the stitching yarn*

preform	length, mm	width, mm	length/width ratio	stitching yarn width, mm	loop height, mm	loop width, mm
dry, face	6.95±1.21	1.42±0.17	4.88	1.09±0.28	–	–
dry, back	6.60±1.19	0.74±0.11	8.92	0.87±0.18	5.00±0.81	3.61±0.54
cured, face	3.71±0.77	0.84±0.13	4.42	–	–	–
cured, inner	3.56±0.79	0.87±0.16	4.10	–	–	–
cured, back	3.95±0.79	0.81±0.25	4.88	0.85±0.23	4.87±0.85	3.22±0.39

Composite plates (stitched and non-stitched) are manufactured using the liquid resin (toughened epoxy) infusion. The final thickness is 5.32 mm that gives the average fibre volume fraction (V_f) of 58% (without taking openings into account). Several pieces are inspected with an optical microscope for details of the internal structure. Typical micrographs of the stitching sites are shown in Fig. 3(left). Measured dimensions are listed in Table 1, which reveals significant (about 50%) reduction in the size of the openings if compare with the dry preform. This effect should be attributed to severe densification of the fibrous plies in the mould (thickness in the dry state is about 9 mm). Taking an average rhomboid 3.6×0.9 mm opening, it can be estimated that V_f in plies after the stitching is 62%, and the openings occupy 6.5% of the total volume.

The widths of the inner and surface openings are almost the same. This disagrees with other materials [2] which show wider surface openings, since the yarn loop bends at the face and backside and, therefore, pushes away the fibres more than in the inner plies. In the present case the small difference can be due to severe compression in the mould.

A prominent nesting of the plies can be observed in Fig. 3(right), where the ply waviness amplitude sometimes exceeds the average ply thickness (5.32/28=0.19 mm). This effect should also be attributed to the out-of-plane compression in the mould.

In the impregnated state, the yarn loop width at the face side is not measured due to roughness of this surface; a smooth surface appears only after polishing out a relatively thick layer including almost all yarn material. As for the backside, it is interesting that the moulding changes the yarn width not very much, probably due to its twist.

The material properties — Young's modulus, E, Poisson's ratio, ν (theoretically estimated for the transversal direction), ultimate tensile stress, σ_{ult}, etc. — are listed in Table 2.

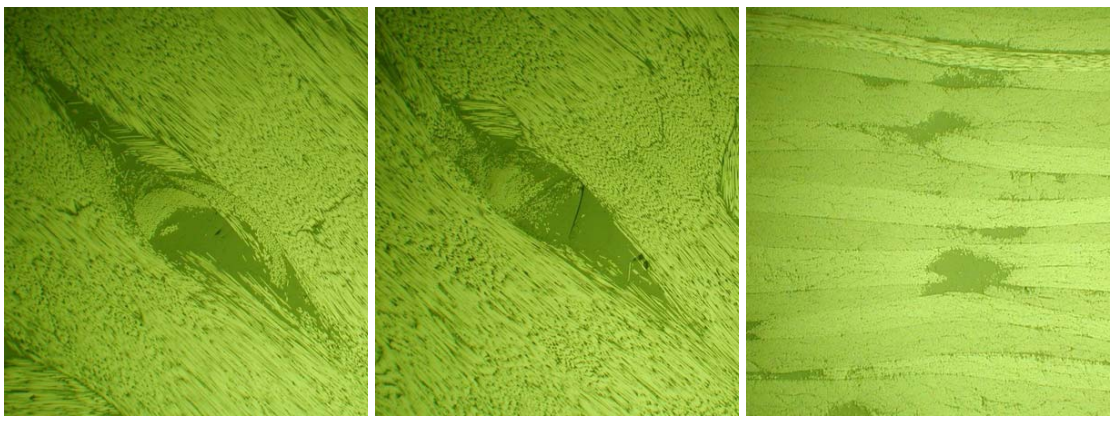

Figure 3: Typical micrographs of inplane (left; layer 5) or cross-sections (right).

Table 2: *Properties of the composite constituents (longitudinal / transversal)*

	material	fibre ∅, μm	twist t/m	density, g/cm^3	lin.dens. tex	E, GPa	ν	σ_{ult}^{tens}, MPa
ply	Tenax IMS 5131	5	0	1.80	820	290/14	0.236/0.011	5600/–
ply	Priform ST54/2Z	30	Z2	1.24	54	2.48	0.3	70.2
stitch	Tenax HTA 5241	7	S15	1.76	67	238/14	0.230/0.014	3950/–
resin	Cycom 977-2	–	–	1.31	–	3.52	0.3	81.4

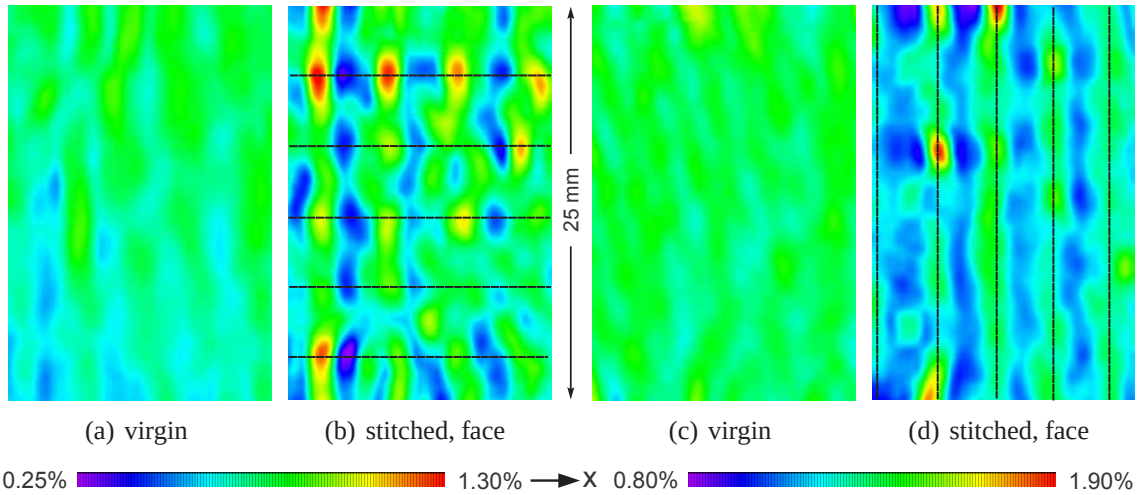

Figure 4: Surface strains ε_x under loading in 0° (a,b) and 90° (c,d) directions. The load is applied in x-direction. The average strain level is 0.75% or 1.35%, respectively. The presumable positions of the stitching yarns are shown with black lines.

3. EXPERIMENTAL

Uniaxial tensile tests are performed according to ASTM D3039; i.e., specimens having a constant 5.32×30 mm cross-section are used. Series of 6 specimens are tested for 0° (along the structural stitching) and 90° directions, at the cross-head displacement rate of 3 mm/min. The tests are monitored with the acoustic emission (AE) and full-field strain registrations. Since the AE sensors should be removed before the specimen failure, the loading is not completely monotonical but is paused at a certain load level.

Figure 4 shows typical strain fields at the face side of different specimens. It is seen that the tufting causes prominent strain concentrations at the stitching sites, in comparison with the non-stitched specimens. For some specimens loaded in 90° direction, analysis of the strain history in such local maximums reveals almost constant strain rate until a moment, when it starts to increase rapidly. This moment can be attributed to the damage onset; afterwards, the local strain more and more differs from the average one. For example, the specimen shown in Fig. 4(c,d) fails at the average strain of 1.57%, while the ultimate local strain approaches 2.5%; the rapid increase starts at about 1.1% of the average strain (the stress level of about 400 MPa). However, it is difficult to say if it is the damage driving the final failure or not; future X-ray investigation should clarify this.

Figure 5(right and centre) shows the cumulative energy of events recorded with the AE equipment. The damage onset is seen already at the beginning of the tests, when a

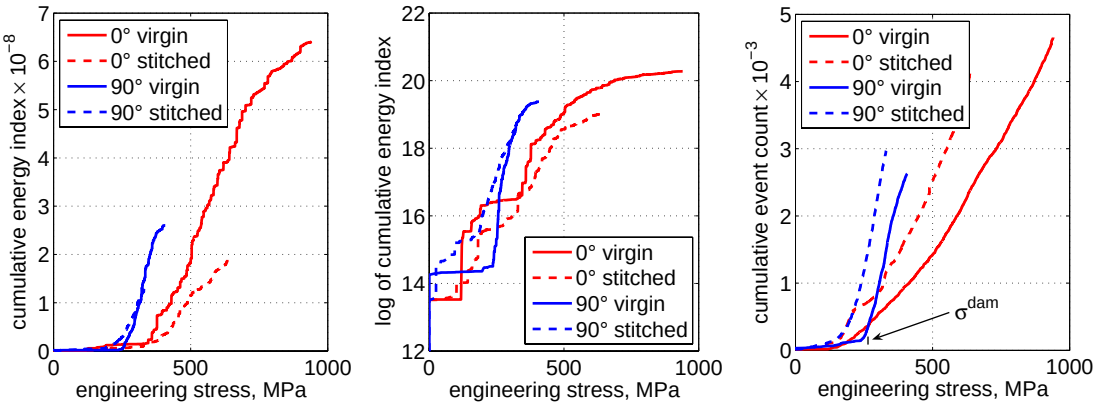

Figure 5: AE energy in normal (left) and logarithmic (centre) scales. Right - cumulative sum of AE event counts.

few low-energy events occur with low frequency. At a certain moment, the frequency increases, the energy content rises quickly, and the specimens starts to emit popping sounds indicating appearance of relatively large cracks (since this occurs at different stresses for 0° and 90° specimens, the sounds are not due to a tab cracking). This should be attributed to a mass microcrack formation, presumably in the off-axis plies; corresponding stress level is denoted further as σ^{dam}. Under 0° loading, this mass cracking starts at the stress level of about 160 MPa both for the non-stitched and stitched specimens, while for 90° loading the stress levels differ significantly (250 vs. 120 MPa).

The clearest picture of the material behaviour is given by the cumulative sum of AE event counts, Fig. 5(right). A drastic change of the curve slope is seen at σ^{dam} level. It is also interesting to note that the event curves have two almost linear parts; this means that the increase of the event number is almost constant within each part.

Similar behaviour is observed for the Poisson's ratio, Fig. 6, which also shows a distinct change at about the same transition strain as the AE curves. Before this threshold, the plots show a wide variation; its reason is still not clear for the authors. After passing the threshold, the Poisson's ratio is more conformable within each test series and keeps almost constant magnitude as the axial strain increases.

Table 3 summarizes the measured mechanical properties: the Poisson's ratios (averaged in the strain range 0.05–0.3%) and Young's moduli, as well as σ^{dam} level, Fig. 5(right). The standard deviations do not exceed 15%.

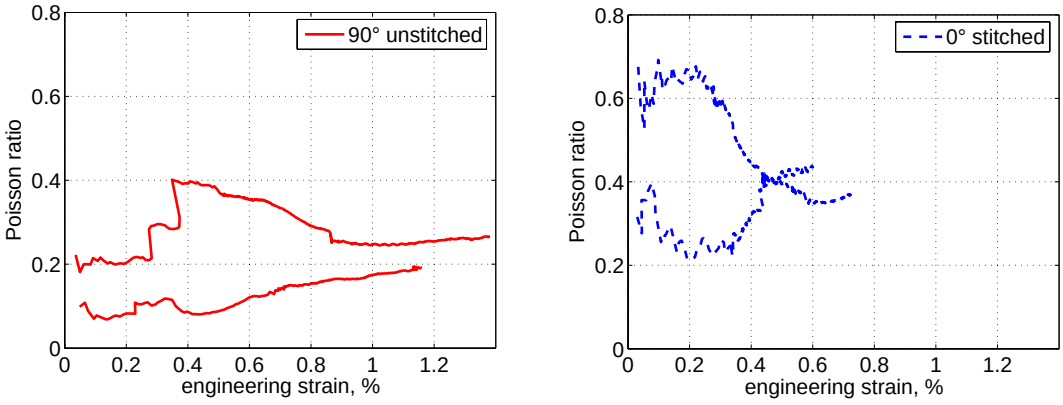

Figure 6: Poisson's ratio variation during the loading.

Table 3: *Homogenized mechanical properties of the composite (mean values, non-stitched / stitched). The moduli are given in GPa, stress — in MPa.*

	E_0	E_{90}	E_z	$G_{0,90}$	$\nu_{0,90}$	$\nu_{90,0}$	σ_0^{dam}	σ_{90}^{dam}
test data	73.4/87.7	46.9/38.9	–	–	.271/.353	.249/.161	148/174	247/120
TexComp	93.6/94.5	49.6/50.2	7.5/8.6	24.0/24.2	.338/.337	.179/.179	–	–
FE	88.9/86.2	46.3/44.7	8.0/8.5	21.8/21.2	.368/.374	.192/.194	–/165	–/140
FE*	85.7	44.9	8.0	21.0	.372	.195	250	140

* with opening but without stitching yarn

4. GEOMETRICAL MODELLING

The preform model is built using StitchTex software, which is a stand-alone application based on WiseTex approach to the generalized textile description [6]. Thus, StitchTex is integrated with existing geometrical and mechanical models of the relaxed or deformed 2D and 3D woven, 2- and 3-axial braided, weft-knitted, and non-crimp warp-knit stitched fabrics, and laminates built on their base. The integration with WiseTex allows also for a direct use of the existing software solutions for the modelling of a resin flow through the reinforcement, micro-mechanical calculations of the composite properties, micro-macro analysis of a composite part, FE models, and virtual reality visualization [6].

The present model is an inevitable simplification of the actual internal structure; e.g., it does not account neither for heavy nesting nor for deplanation of the plies caused by consolidation in the mould, Fig. 3(right). It is obvious that a semi-analytical approach can not mimic such features, which are hardly modelled even in an FE analysis.

First, consider the fabric model, which is built with the thickness of 0.19 mm (the laminate thickness divided by 28 plies) and parameters listed in Section 2. To achieve the best agreement with the nominal total areal weight of the fabric, a denser structure is modelled for the carbon yarns (0.117×3.9 mm cross-section). The polysulfone yarn width is also accepted a little smaller than the measured one: the cross-sectional size is 0.115×0.19 mm (along carbon yarns) or 0.024×0.9 mm (across them).

The model is built easily with WiseTex but absence of nesting results in a too high local V_f inside the yarns; it even slightly exceeds 100% (in reality these "excess" fibres fill the voids between the yarns and plies due to nesting and distortion of the yarn shapes). If, other way round, the yarn thicknesses are chosen to give a reasonable V_f, then the ply thickness is overestimated, and the overall V_f is underestimated. Since the correct V_f is crucial for method of inclusions used further to calculate the homogenized stiffness matrix, the latter way (with a realistic V_f inside yarns) is adopted. Then, the geometrical model is created with the thickness slightly larger than the nominal one and local V_f of about 90% (below the ultimate packing case of 90.7%) inside the yarns. The warp and weft crimp is chosen to minimize the fabric thickness for the given yarn dimensions.

The model of the reinforcement fabric is shown in Fig. 1(right).

The preform model is built by 1) multiplication and rotation of the ready fabric model exported from WiseTex and 2) appending the stitching loops (optionally). The following simplifying assumptions are accepted to produce a physically sound and computationally feasible model sufficient for a correct estimation of the homogenized properties:

- as already noticed above, no nesting is modelled. The preform is a stack of flat plies, which have equal uniform thickness, and their bounding boxes do not intersect;

- the openings are not modelled, since a) WiseTex approach does not allow to split a yarn and b) the openings have a negligible effect on the homogenized stiffness [7]. Thus, there are interpenetrations of the stitching and fabric yarns but this does not matter for the physical model used further (method of inclusions);
- the piercing pattern is regular (constant stitching length and distance between seams). This is a reasonable simplification for a well-controlled robot process, although some irregular scatter can be observed even in such an "ideal" case [2, 3];
- seams are straight (no zig-zag offset of the piercing pattern) and parallel. No initial shift is assumed between them (i.e., a rectangular piercing pattern is produced);
- the stitching yarn consists of a single strand (in reality, it can be composed of several twisted strands). This assumption is accepted due to a strong randomization of the strand positions and shapes along the yarn path [2];
- the cross-section is circular along the through-the-thickness yarn path. The yarn flattening is optionally modelled only at the preform surface, to avoid segmentation of the surface plies in an FE model (since the yarn diameter can exceed the ply thickness, and the latter can be cut if the yarn is sunk into the preform). The cross-sectional area is preserved constant along the yarn (just to simplify the FE model);
- the through-the-thickness yarn path is either straight or helical (spiral built around an imaginary straight line). In reality, it can be inclined due to a local deformation of the preform during the stitching, draping, compression in the mould, etc. This can play a role for the out-of-plane stiffness but is difficult to be accounted for without an unnecessary complication of the model;
- elastic yarn bending is assumed in some cases; in other cases, the yarn bent shape is defined reasoning from purely geometric considerations (straight lines, arches);
- the backside loops are placed regularly. Their height is equal and a little reduced if compare with the measured one. This allows avoiding interpenetrations of the stitching yarns that is important for the FE model discussed in the next Section.

The geometrical models of the stitching loop and stitched preform are shown in Fig. 7. In the latter case, for better visualization, the stitching loops are not sunk and flattened.

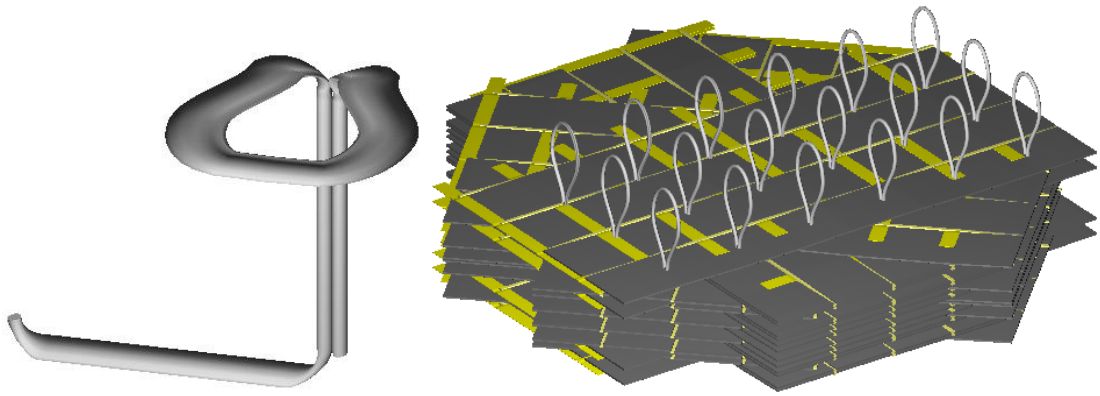

Figure 7: Models of the stitching loop repeat (left) and stitched preform (right).

To calculate the homogenized elastic properties, the method of inclusions [8] is used, which is implemented in TexComp software. In the computational scheme, the model thickness is reduced artificially to achieve the nominal one (5.32 mm), thus "nesting" the inclusions into the volume having the correct average V_f.

Table 4: *Material properties estimated using the Chamis' formulae (moduli are in GPa)*

	V_f, %	E_L	E_T	E_Z	G_{LT}	G_{TZ}	G_{ZL}	ν_{LT}	ν_{TZ}	ν_{ZL}
ply, no openings	58	168.5	8.6	7.2	5.7	2.3	2.8	0.255	0.373	0.012
ply, with openings	62.1	180.0	9.0	7.5	6.0	2.5	3.0	0.253	0.361	0.013
stitching yarn	90.7	216.0	11.7	11.7	73.3	4.7	73.3	0.234	0.237	0.013

Results are listed in Table 3 and are in a good agreement with the experimental data. The difference can be due to natural reasons: 1) inaccuracy in the material properties (which can differ a little from the nominal values) and 2) neglected deplanation and nesting of the plies. There is also an error inherent for the homogenization procedure; particularly, it assumes no free surfaces, while the laminate thickness is limited.

5. FE MODELLING

The meso-level FE analysis (meshing of the laminate and stitching yarn volumes, mesh superposition technique) is performed using MeshTex/Sacom/M3 softwares [9].
To decrease the computational costs, it is interesting to access the influence of the stitching yarn and openings on the FE results; the stitching loop is quite complex, and if it is possible to obtain reasonable estimations of the composite properties without the stitching included, e.g. as done in [10], then pre-processing of the FE model can be much easier. Thus, the FE analysis is performed for several models of different complexity: 1) only laminate without stitching and openings, 2) without stitching but with openings, and 3) with stitching and openings. In the last two variants, the local fibre re-orientation around the openings is accounted for also, following the procedure proposed in [7]. Both the opening an area of misaligned fibres are modelled as ideally rhomboidal.
For simplicity, textile structure of the plies is neglected, and they are modelled as UD mats having the same average V_f of the carbon fibres as the initial fabric. This is a reasonable simplification due to compact placement and a low crimp of the carbon-fibre tows in the relaxed fabric. Polysulfone yarns are not modelled also, since their stiffness and strength are similar to these of the matrix material, Table 2. The homogenized orthotropic properties are determined using the Chamis' formulae, Table 4.
The stitching loop is meshed using the centerline coordinates and cross-sections imported from StitchTex geometrical model described above, Fig. 7(left). As noticed in the previous

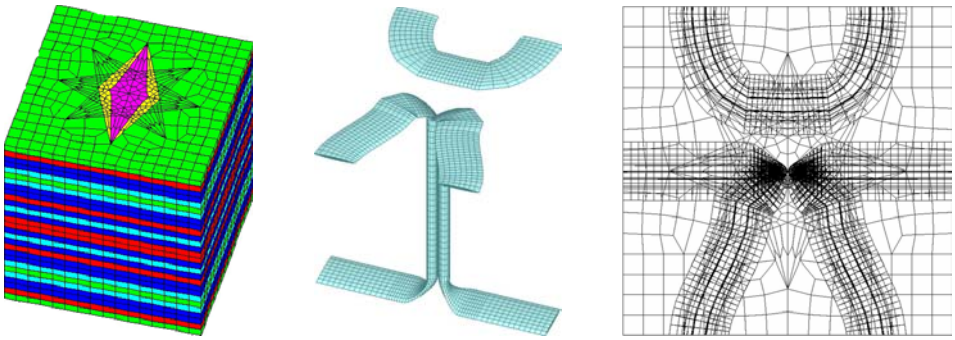

Figure 8: FE mesh of the laminate and stitching loop (5312 elements in total). For the backside ply, the opening is shown in pink, and the area of re-oriented fibres — in yellow.

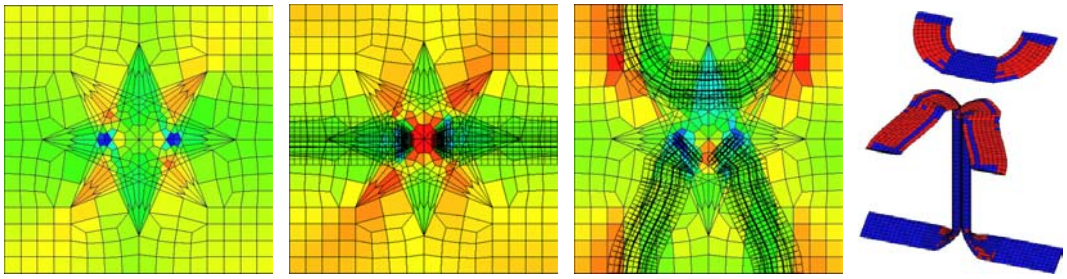

(a) no stitching (b) stitching, face (c) stitching, back (d)

Figure 9: Typical stress distributions (a–c, σ_0) and damaged elements in the yarn loop (d, mode T&LT, marked red) under loading in 0° direction at 0.1% average strain.

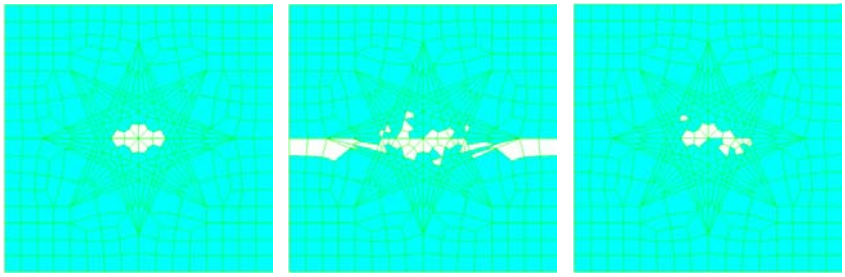

(a) no stitching (b) face, stitching (c) back, stitching

Figure 10: Damaged elements in the surface plies (mode L, marked white) under loading in 90° direction at 0.8% average strain.

Section, the cross-sectional area is preserved to be constant along the stitching loop, and only the shape changes (ellipse with different axes ratio).
The FE models of the laminate and stitching loop are shown in Fig. 8. To fit $5\times5\times5.32$ mm unit cell, the backside loop of the stitching yarn is meshed in two parts. Periodic boundary conditions (translation symmetry of the unit cell) are applied in the model plane.
To obtain the elastic properties, the model is sequentially loaded in 0° and 90° directions by applying 0.1% strain. Results are given in Table 3 along with the test data and theoretically estimated values; they are in a good agreement. Typical stress distributions are shown in Fig. 9. It is seen that the opening results in a prominent disturbance of the stress field; introduction of the stitching loop causes even greater stress concentrations. However, the effect on the stiffness matrix in very small, less than 3%. The exception is the out-of-plane stiffness, which rises in 7% if the stitching loop is superimposed.
The damage onset and propagation are calculated also, using the Hoffman's criterion; the damage mode is set by the maximum value among the corresponding stress-to-strength ratios. It is obtained that the stitching loop triggers the damage onset, which appears earlier than in the case with the opening but without the loop. The damage growth is also more extensive in the former case as revealed by Fig. 10. The damage onset stresses are given in Table 3 and are in a good agreement with the test data.

6. CONCLUSIONS

This paper deals with a case study of the meso-level geometrical and FE modelling of a structurally stitched woven laminate. The main results are

- the structural stitching produces a negligible influence on the in-plane components of the homogenized stiffness matrix. Accounting for the stitching loop is important only for the transversal stiffness and related constants. Thus, relatively simple models without openings can be used to obtain the stiffness matrix;
- however, the stress-strain fields are sensitive to a local geometry, which can play the role of a stress concentrator and trigger damage. Therefore, presence of the stitching yarn and openings, as well as specifics of their modelling is important for a correct computation of the damage onset and propagation. Of course, word "correct" should be understood here in a relative sense due to a strong randomization of the micro- and meso-level internal structure of a real composite;
- for a typical structurally stitched composite, FE simulation results and theoretical estimations (method of inclusions) are compared with experimentally measured properties. They agree well thus showing efficiency of the developed models.

7. ACKNOWLEDGEMENTS

The work reported here is done within I-TOOL ("Integrated Tool for Simulation of Textile Composites") project funded by the European Commission. Ms. Solange Amouroux and Mr. Arnaud Alix (Dassault Aviation, France) are gratefully acknowledged for supplying the composite material. Authors would also like to thank Mr. Kris Van de Staey and Mr. Paul Crabbé (Dept. of Metallurgy and Materials Engineering, K.U.Leuven) for assistance with the mechanical testing and polishing equipment.

REFERENCES

1. Åström, B.T., "Manufacturing of polymer composites", Chapman & Hall, 1997.
2. Koissin V. et al, "Internal structure of structurally stitched NCF preform", *Proc. of 12th European Conference on Composite Materials (ECCM-12), Biarritz, France, August 29 — September 1, 2006.* CD-edition.
3. Koissin V. et al, "On-surface fiber-free zones and irregularity of piercing pattern in structurally stitched NCF preforms", *Advanced Composites Letters*, 2006;**15**(3):87–94.
4. "Priform UW 200 IMS G 24K 100 Specification", Cytec Eng. Materials Inc., USA, 2005.
5. "Delivery programme and characteristics for Tenax filament yarn", Toho Tenax Europe GmbH, Germany.
6. Verpoest I. and Lomov S.V., "Virtual textile composites software WiseTex: integration with micro-mechanical, permeability and structural analysis", *Composites Science and Technology*, 2005;**65**(15–16):2563–2574.
7. Koissin V., Lomov S.V., and Verpoest I., "Uneven fibre distribution in structurally stitched NCF preform: FE modelling", *Proc. of 22nd Int. Conference on Boundary and Finite Element Methods (BEM-FEM-22), St.Petersburg, Russia, September 26–28, 2007.* CD-edition.
8. Lomov S.V. et al, "Textile composites: Modelling strategies", *Composites Part A*, 2001;**32**(10):1379–1394.
9. Nakai H., Kurashiki T., and Zako M., "Individual modeling of composite materials with mesh superposition method under periodic boundary condition", *Proc. of 16th Int. Conference on Composite Materials (ICCM-16), Kyoto, Japan, July 8–13, 2007.* CD-edition.
10. Heß H., Roth Y.C., and Himmel N., "Elastic constants estimation of stitched NCF CFRP laminates based on a finite element unit-cell model", *Composites Science and Technology*, 2007;**67**(6):1081–1095.